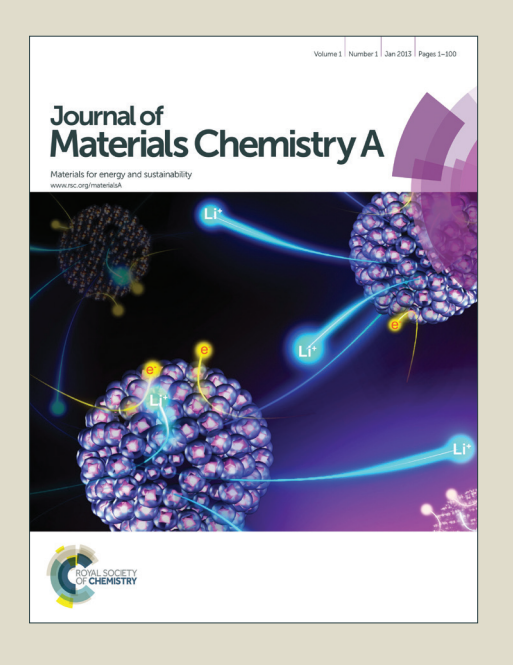
Journal of Materials Chemistry A

Accepted Manuscript



This is an *Accepted Manuscript*, which has been through the Royal Society of Chemistry peer review process and has been accepted for publication.

Accepted Manuscripts are published online shortly after acceptance, before technical editing, formatting and proof reading. Using this free service, authors can make their results available to the community, in citable form, before we publish the edited article. We will replace this Accepted Manuscript with the edited and formatted Advance Article as soon as it is available.

You can find more information about *Accepted Manuscripts* in the **Information for Authors**.

Please note that technical editing may introduce minor changes to the text and/or graphics, which may alter content. The journal's standard <u>Terms & Conditions</u> and the <u>Ethical guidelines</u> still apply. In no event shall the Royal Society of Chemistry be held responsible for any errors or omissions in this *Accepted Manuscript* or any consequences arising from the use of any information it contains



RSCPublishing

ARTICLE

Ammonia borane-polyethylene oxide composite materials for solid hydrogen storage

Cite this: DOI: 10.1039/x0xx000000x Received 00th January 2012,

Accepted ooth January 2012

DOI: 10.1039/x0xx00000x

www.rsc.org/

A. S. Nathanson ^a, A. R. Ploszajski ^a, M. Billing ^a, J. P. Cook ^b, D.W. K. Jenkins ^c, T. F. Headen ^b, Z. Kurban ^b, A. Lovell ^b and S. M. Bennington ^b

Co-electrospinning ammonia borane (AB) and polyethylene oxide (PEO) has created a unique crystal phase that promotes faster hydrogen release from AB below its melting temperature with no incubation time. Integral fibres have been produced containing 75%, 50% and 25% AB by weight. As the PEO content was increased, the onset temperature of dehydrogenation was reduced from 110°C for pristine AB to 85°C for the 25% AB fibres. The new phase is characterised by hydrogen bonding between the hydridic hydrogen atoms bonded to the nitrogen atom in AB and the oxygen atom in the PEO backbone. Additionally, the usual foaming of AB during hydrogen release was effectively controlled by the addition of PEO. Some impurities which accompany the hydrogen release - ammonia and diborane - are reduced, however, borazine levels in the gas stream were observed to increase during the loss of the 2nd hydrogen equivalent. Nevertheless, co-electrospun composites of AB and PEO show great promise as a safe, portable and versatile hydrogen storage material.

Introduction

In recent years the complex hydride ammonia borane (NH₃BH₃, AB) has become one of the most promising candidates for solid-state hydrogen storage with the potential to meet the targets set out by the US Department of Energy (DOE) for on-board hydrogen storage technologies ^{1,2}. AB has a high hydrogen content of 19.6% hydrogen by weight, two thirds of which can be released below 200°C ^{3–5}, and is particularly attractive on account of its low toxicity, solubility in many common solvents and good stability in both air and moisture ¹.

Hydrogen is released from AB in discrete steps, activated by temperature, consisting of the 1st, 2nd and 3rd hydrogen equivalents from each AB molecule. During the three steps AB transforms progressively into polyamidoborane (PAB), polyimidoborane (PIB) and finally boron nitride (BN).

$$nNH_3BH_3 \xrightarrow{90^{\circ}C-200^{\circ}C} (NH_2BH_2)_n + nH_2$$
 (1)

$$(NH_2BH_2)_n \xrightarrow{120^{\circ}C - 500^{\circ}C} (HNBH)_n + nH_2 \quad (2)$$

$$(HNBH)_n \xrightarrow{>500^{\circ}C} nBN + nH_2$$
 (3)

These steps are sequential but overlapping; before the entire 1st equivalent of hydrogen has evolved the second step will have begun ^{5,6}. Hydrogen evolution follows sigmoidal kinetics, indicative of a nucleation and growth mechanism. The general reaction scheme hides much complexity as AB can polymerise to form chains or cyclise to rings, which leads to the release of the gaseous impurity borazine ^{7,8}.

Despite its potential, the widespread utilisation of AB is impeded by some critical issues such as a long incubation period prior to hydrogen release (lasting 2 hours at 85°C), the production of foam upon decomposition, the generation of toxic, volatile gaseous by-products including ammonia and borazine, and poor reversibility ^{2,5,9–11}, although recently success has been reported for the regeneration of AB by a chemical digestion with liquid ammonia and hydrazine ¹².

To overcome these issues, a number of different strategies have been investigated, from the nanostructuring of AB within scaffold materials 13-18, the addition of metal-containing compounds ^{19–22}, and various non-metal additives ^{23–27}. Polymers in particular hold great promise as additives since they are, in general, inexpensive, widely available, lightweight and can be synthesised to contain a variety of chemical moieties. In fact, a number of studies have shown that polymers are effective as promoters of hydrogen release from AB. AB blended with polyacrylamide (PAA) ²⁸, AB-polymethylacrylate (PMA) composites ²⁹, electrospun AB co-fibres with polystyrene (PS) and polyvinyl pyrrolidone (PVP) 30 showed significantly improved dehydrogenation properties compared to pristine AB with a lower onset temperatures and no incubation period. However, the AB contents achieved were low and the issue of foaming was not addressed. Additionally, the PAA and PMA containing materials showed complete suppression of boroncontaining impurities and increased ammonia evolution.

In this study, electrospinning ³¹ is employed for the fabrication of the first solid-state AB-polymer composite materials based on a polyether, polyethylene oxide (PEO). Herein it is reported that these composite materials exhibit enhanced hydrogen release properties compared to pristine AB, with reduced hydrogen

release temperatures, faster hydrogen release kinetics and reduced foaming. It is believed that such materials have great potential as low cost, safe hydrogen storage solutions.

Experimental

Materials

Ammonia borane (AB, 97%), polyethylene oxide (PEO, M_v ~2,000,000) and acetonitrile (ACN, anhydrous, 99.8%) were purchased from Sigma Aldrich and used as-received.

Electrospinning of AB-PEO fibres

In a typical experiment, the electrospinning solution was prepared by the addition of AB to a solution of PEO, 3 wt% in ACN. The solution was pumped through a steel nozzle (inner diameter 0.46mm) at a rate of 1 ml/hr, set using a Harvard PHD2000 syringe pump, and fibres drawn onto an aluminium foil collection plate approximately 30 cm away, under a potential of 12 keV. The procedure was performed at room temperature and pressure in a fume hood. A schematic of the electrospinning apparatus can be seen in Fig. 1. and further information about the electrospinning process is available in the supplementary information.

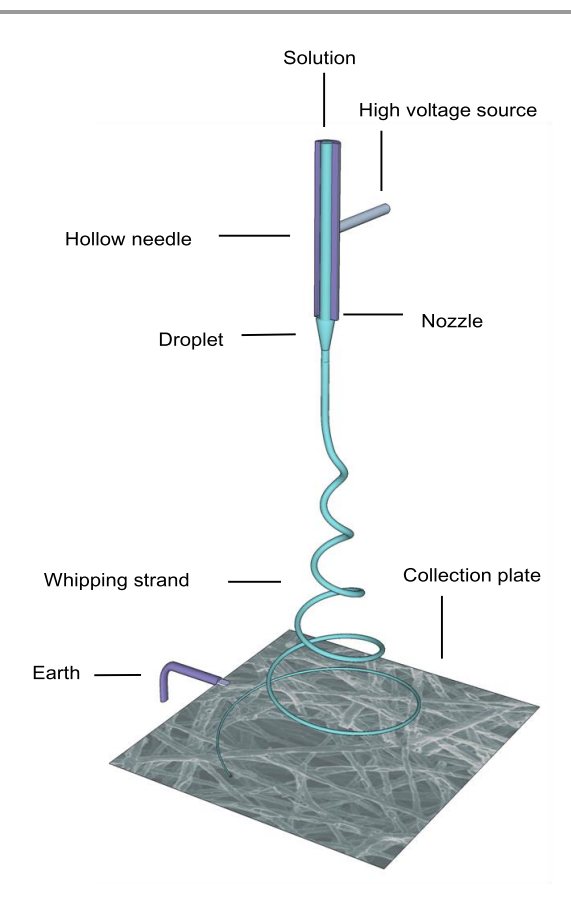


Fig. 1 Cut-away schematic of the single-phase electrospinning setup.

For this study, samples were prepared with AB contents of 25, 50 and 75wt% (with respect to the total mass of AB and PEO in the spinning solution). The gravametric hydrogen content that can be released below 200 °C for the three materials is 3.3, 6.5 and 9.8 wt% respectively. For convenience, the composite materials produced (AB-PEO fibres) will be referred to as AB25, AB50 and AB75 respectively hereafter.

Analysis

The morphologies of the AB-PEO fibres were examined by scanning electron microscopy (SEM) using a Hitachi Tabletop Microscope TM 1000, a FE-SEM Hitachi S4000 and a Jeol JSM-6480LV instrument.

X-ray diffraction (XRD) was employed to investigate the microstructure of the as-prepared composite materials and was performed on a Phillips X'pert Xray diffractometer (Cu K α radiation, wavelength 1.5418 Å).

The dehydrogenation properties of the materials were analysed using thermogravimetric analysis (TGA) and differential scanning calorimetry (DSC), performed using a Mettler Toledo combined TGA-DSC system, the TGA/DSC 1. A quadrupole MKS Cirrus 2 atmospheric pressure residual gas analyser (RGA) was used to analyse the volatile species released from the TGA-DSC instrument. TGA-DSC-RGA experiments were performed using a ramp heating regime between 35°C and 200°C with a heating rate of 2°C min⁻¹, and step heating regimes to 80°C, 100°C and 120°C. Three samples of each material were tested to ensure consistency.

The foaming response of the pristine AB and the AB-PEO materials was observed by warming small pellets of mass approximately 1 g in an oil bath at 120 °C for 3 minutes. The pellet dimensions were measured before and after heating and the expansion calculated as a percentage difference of the final foamed pellet to its initial size.

In situ solid-state ¹¹B magic angle spinning nuclear magnetic resonance (MAS-NMR) spectroscopy was performed on AB and AB50 using a Varian VNMRS 400 spectrometer at 128.3 MHz and a 4mm (o.d.) rotor. Spectra were obtained during isothermal experiments at 85°C using cross-polarisation with a 1.0 s recycle delay, 40 ms contact time and at a sample spin-rate of 10 kHz. Between 20 and 100 repetitions were accumulated. Spectral referencing was performed with respect to an external sample of F₃BOEt₂.

Solid-state ¹⁵N MAS-NMR was performed on the AB50 sample. The spectra were recorded at 40.527 MHz using cross-polarisation with a 5.0s recycle delay, 40 ms contact time and at a sample spin-rate of 6.8 kHz. Spectral referencing was performed with respect to an external sample of CH₃NO₂.

Attenuated total reflection Fourier transform infrared spectroscopy (FTIR) was performed using a Bruker Optics Vertex 70 spectrometer (633 nm laser, 1 cm⁻¹ resolution). FTIR was used to analyse the as-prepared materials and samples which had been heated in an oil bath at 85°C for up to 120 min followed by rapid cooling in an ice-water bath to quench any further

reactions. The peak positions were determined by fitting

Gaussian distributions to the spectra.

Results and Discussion

Structure of electrospun materials

An example of as-electrospun AB-PEO material is shown in Fig. 2. The material produced was fibrous, resembling cotton wool. The SEM images in Fig. 2 showed the fibres to be rough but integral and roughening as the AB content was raised. Some fusion at intersections was observed suggesting incomplete drying during spinning. To remove any residual solvent, the fibres were left to dry under extraction in a fume hood for 24 hours. The diameters of all the fibres produced are consistently in the 2-5 µm range. No obvious crystals of AB were present.

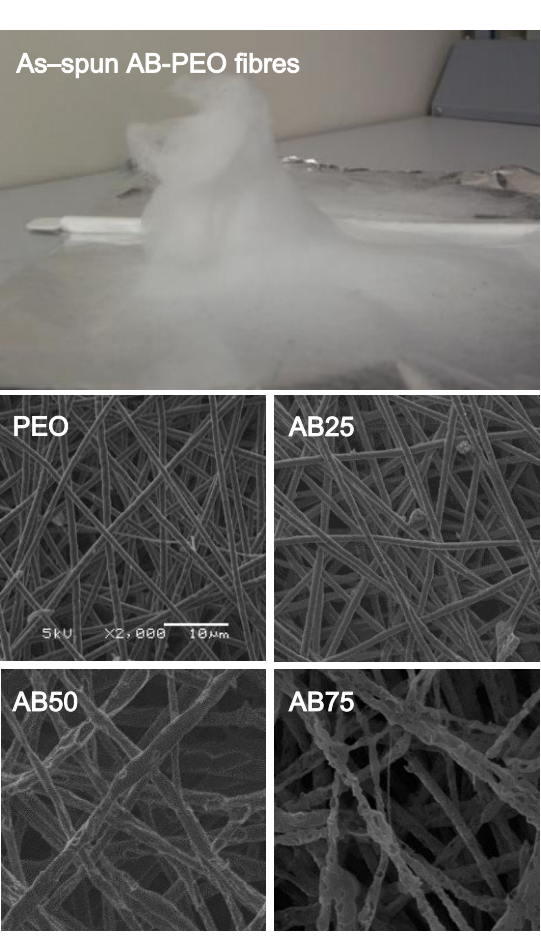


Fig. 2 AB-PEO fibres with different amounts of AB, as the ratio of AB to PEO increases the fibres become rougher.

AB adopts a tetragonal unit cell at ambient temperatures and the most prominent of its XRD peaks are the (110) and (101) reflections, at 24.0° and 24.5° respectively 32. PEO is a semicrystalline material with monoclinic crystalline domains, the intense XRD peaks are the (120) and (112) reflections at 19° and

23.2° respectively ³³. Tetragonal AB peaks were observed in AB75 and AB50, but not in the AB25 sample, which suggests that bulk AB phases are present only in the high AB-content materials. The main PEO peaks disappear in the AB-PEO fibres, suggesting that significant changes have occurred in the structure of the PEO during electrospinning with AB.

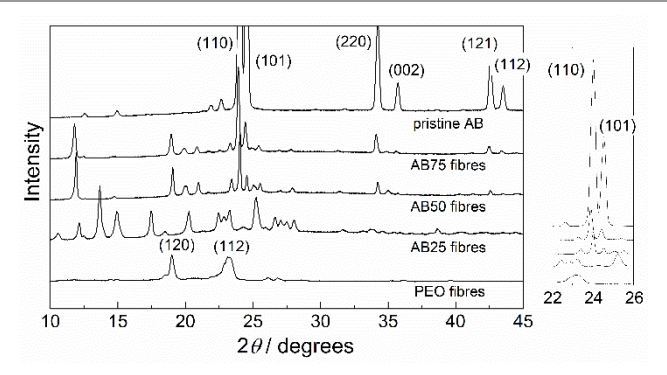


Fig. 3 X-ray diffraction pattern of AB, PEO granules and the electrospun fibres.

New peaks are also observed at 10.6°, 12.1°, 13.4°, 14.9°, 18.3°, 20.0° and 25.2° 2θ, which suggests the formation of a mixed phase, distinct from both AB and PEO. The diffractogram of the AB25 material is again different from the fibres with higher AB content. It seems reasonable to expect that AB and PEO would mix due to their polar nature and the new XRD peaks observed are likely a mixed AB-PEO phase. Further analysis of this mixed AB-PEO phase is currently ongoing.

Dehydrogenation of AB in the electrospun fibres

The dehydrogenation properties of the materials were investigated using a combined TGA-DSC-RGA system. The DSC data were normalised to the total sample mass and the TGA data were normalised to the nominal AB content, as there was no appreciable mass loss from the polymer (total sample mass loss data is available in the supplementary information). The RGA data were normalised to the total cumulative hydrogen RGA signal. The gas stream impurity content was calculated as a factor of the total hydrogen release. However this assumption that the normalised RGA signal output scales linearly with the initial mass of the measured sample was only observed as true when the sample masses were similar. Thus, the composites compare well with each other (~8 mg) and poorly to the pristine AB (~1 mg) the excessive foaming of pristine AB meant that only a small quantity could be tested.

The RGA trace of the hydrogen release from AB (Fig. 4i) shows two peaks, the 1st and 2nd hydrogen equivalents, at 110°C and 150°C respectively, in accordance with literature ^{25,34}. The addition of PEO to AB was found to successively decrease the temperature at which each hydrogen release step occurs. The centre of the first hydrogen release peak is found to decrease to 105°C, 102°C and 98°C for AB75, AB50 and AB25 respectively. The temperature of the second dehydrogenation peak is also found to decrease upon addition of PEO, with AB75, AB50 and

AB25 samples exhibiting peaks centred at 122°C, 120°C and 110°C respectively. It should be noted that the reduction in temperature for hydrogen release is more pronounced for the second step, which leads to overlap of the hydrogen release signals in the RGA traces. This effect is particularly prominent for the AB25 sample which indicates that the presence of PEO is accelerating the reactions in both equations 1 and 2.

ARTICLE

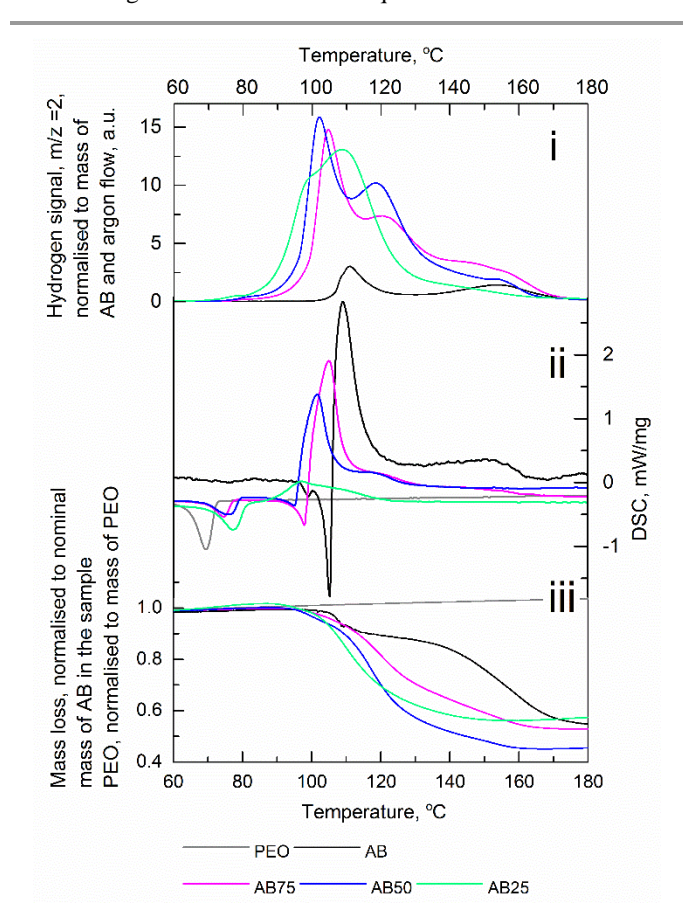


Fig. 4 Combined RGA hydrogen signal, m/z=2, i, DSC, ii and TGA, iii, for pristine AB, PEO and the AB-PEO electrospun fibres; AB25, AB50 and AB75. As the fraction of PEO in the sample increases, the hydrogen release is activated at lower temperatures. Mass loss occurs earlier in AB-PEO composites than in the pristine AB but the final wt% lost is similar (~50%) in both. In the DSC curves, successive addition of PEO reduces the depth of the AB melting endotherm. The earlier release of hydrogen is accompanied by an exotherm which reduces the apparent size of the melting endotherm.

In the DSC curves in Fig. 4ii the exothermic peaks associated with the dehydrogenation of AB correlate exactly with the hydrogen release peaks in the RGA above. Prior to the hydrogen release exotherms, an endothermic process is observed, beginning around 95°C with a minimum at 105°C. This endotherm is attributed to the melting of AB. In the case of the AB-PEO fibres, the depth of the AB melting dip reduces with respect to the height of the hydrogen release peak as the PEO content is raised. This suggests a reduction in the extent of melting of AB in the fibres as compared to pristine AB.

Also present in the DSC data is an endotherm associated with the melting of PEO which begins at 60°C and reaches a minimum at 69°C, consistent with the literature melting temperature of PEO (67°C) ³⁵. The peak minimum is observed to shift to 78.5°C for the AB25 sample and then drop slightly to 76.5°C and then 74°C for the AB50 and AB75 samples respectively. Initially it was assumed that the increase in melting temperature was due to an increase in crystallinity; however, the disappearance of monoclinic PEO peaks in the XRD data makes this unlikely. Most likely, the change in melting temperature is linked to the new AB-PEO phase indicated in the XRD data.

From the TGA data in Fig. 4iii it can be seen that AB loses approximately 50% of its initial mass upon dehydrogenation under this heating regime³⁶, whilst the PEO resists decomposition. We can therefore assume that the mass loss from the materials is entirely the result of mass loss from the AB contained within them. By normalising the TGA data to the nominal AB content of the samples, we can see clearly that the total mass loss from AB within the AB-PEO materials is similar to that of pristine AB, ~50%. However, the rate of mass loss from the fibres is faster and begins at lower onset temperatures than pristine AB. This final mass loss is far greater than the theoretical 13% accounted for by the loss of 2 hydrogen equivalents and suggests that other entities besides hydrogen are being released. It should be noted that the expected release of 2 equivalents of hydrogen from the AB-PEO materials represents a conservative estimate, since more than 2 equivalents are in fact usually

In Fig. 5, the hydrogen release of the various samples are shown as a normalised cumulative integral with errors, and the principal impurities borazine, diborane, ammonia and water, are shown as a fraction of the hydrogen signal ^{11,38}. This is a useful method to estimate the species present in the released gas. Water is the principal impurity in the gas stream, and as water is nine times heavier than hydrogen, this could go some way to account for the significant mass loss. Water was not used in processing the composites but it is likely that AB had absorbed ambient moisture³⁹. Acetonitrile was the solvent used in the electrospinning and some residue may have been expected in the fibres; however it was not observed in the RGA data.

1.2 0.0 0.0 0.0 Hydrogen AB N 0.4 **AB75 AB50** N 0.2 AB25 100 200 60 80) 120 140 Temperature, °C 160 180 normalised to hydrogen signal Water Ammonia 0.03 0.15 m/z = 17. to hydr 0.02 0.10 0.05 0.01 0.00 ed to hydrogen signal Borazine Diborane 0.015 0.015 0.010 0.010 m/z = 810.005 0.005 0.000 80 100 120 140 160 180 200 60 80 100 120 140 160 180 200

Fig. 5 Cumulative integrals of the RGA data from the heating ramps of pristine AB and the AB-PEO electrospun fibres; AB25, AB50 and AB75. It is noted that raising the amount of PEO in the mix aids the hydrogen release but produces more borazine. The data was normalised to the hydrogen (m/z = 2) level at 190°C and errors in the data are shown as the lighter background.

Temperature, °C

Temperature, °C

The levels of ammonia, diborane and water in the gas stream remain similar for the three AB-PEO composites whilst the level of borazine increases as the PEO content increases. We can explain this increase with two reasons. Firstly, many previous studies conducted on the dehydrogenation of AB in the presence of etheral compounds: tetrahydrofuran ⁴⁰, glyme ⁴¹, triglyme ⁴² and various polyethers ²³, show accelerated hydrogen release accompanied by significant volumes of borazine. Additionally, borazine is formed during the second hydrogen release step ^{5,8,38}. PEO is an etheral compound and in the AB-PEO fibres the second hydrogen release step occurs at lower temperatures (110 °C) than for pristine AB (145 °C). Therefore, an increased level of borazine release from the AB-PEO fibres is consistent with literature.

In Fig. 6 it can be seen that at each temperature, as the PEO content is raised, the hydrogen release begins at earlier times and progresses at a faster rate. The level of the hydrogen signal also increases with PEO content, a sign of the earlier release of the 2nd hydrogen equivalent observed in Fig. 5.This suggests that the PEO works to reduce the nucleation period of AB to dehydrogenation.

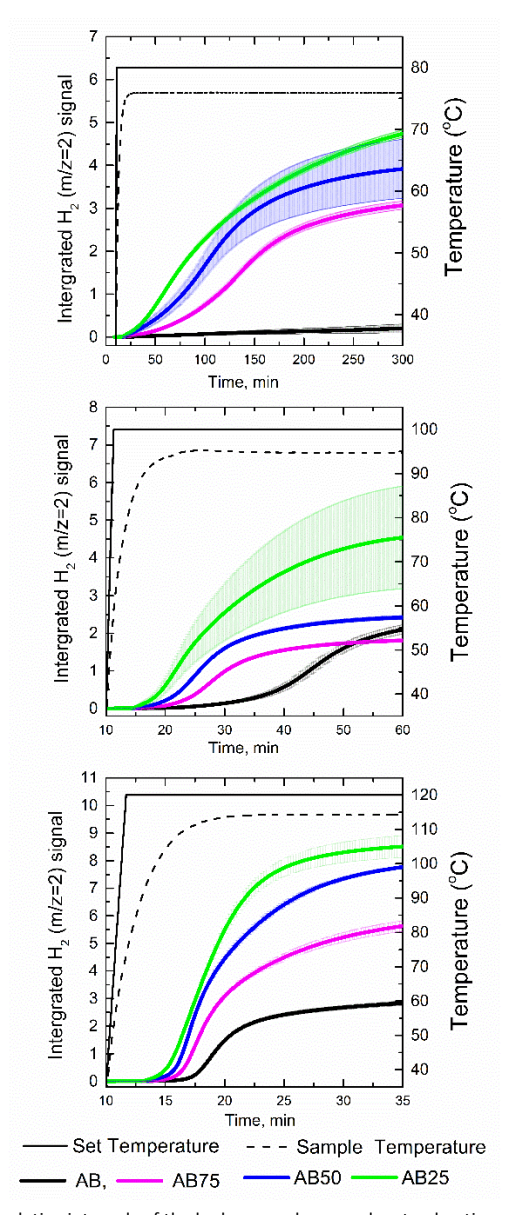


Fig. 6 Cumulative integrals of the hydrogen release under step heating runs of set temperatures 80, 100 and 120°C, of pristine AB and the AB-PEO electrospun fibres; AB25, AB50 and AB75. At each temperature, as the PEO content is raised, the hydrogen release begins at earlier times and progresses at a faster rate. The level of the hydrogen signal also increases with PEO content, a sign of the earlier release of the 2nd hydrogen equivalent.

PEO was found to be highly effective at reducing the foaming of AB in the composites, Fig. 7. This agrees well with the DSC data in Fig. 4ii which show a reduction in the extent of AB melting as the PEO content increases - the presence of less molten AB results in less foam production. However, it was noted that the composites deposit white solids on the container walls upon dehydrogenation, which does not occur for AB. It is believed that these deposits are a mixture of AB-like materials as suggested by Frueh *et al.* ³⁶. The loss of such material will represent a significant contribution to the increased overall mass loss observed for AB-PEO materials.

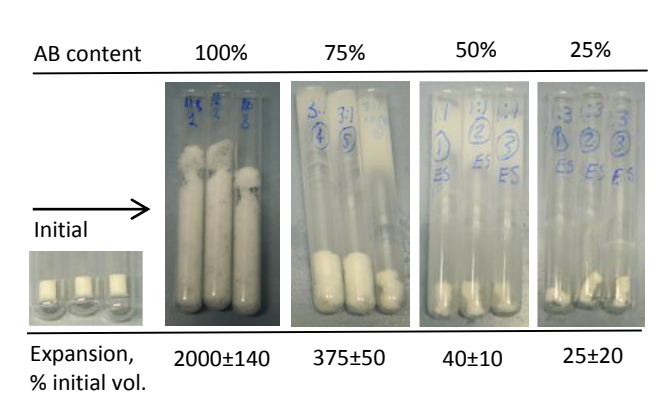


Fig. 7 Foam tests with pellets of electrospun, AB75, AB50 and AB25, and asreceived AB powder. An example of the size and shape of the as produced pellets is shown on the far left. The dehydrogenated materials expansion and foaming is inhibited by the PEO.

Chemical properties of the AB-PEO composite fibres

The SEM, XRD and DSC data suggest that the AB and PEO in the fibres have mixed together on a molecular level to form a distinct phase with properties different from AB and PEO. To gain insight into the chemical nature of this phase, FTIR, ¹⁵N NMR and ¹¹B NMR were performed on the AB-PEO fibres. In the FTIR data in Fig. 8, the pristine AB $^{43-45}$ and PEO 15,46,47 both demonstrated the expected stretches. These peaks are also observed in the spectrum of the AB-PEO fibres; however, some significant changes have occurred. Moving from the AB75 through to the AB25 sample, a successive drop in the AB peak intensity occurs at 1599 cm⁻¹ and 1376 cm⁻¹ (NH₃ symmetric and asymmetric deformations respectively), 1154cm⁻¹ (BH₃ deformation) and at 1056cm⁻¹ (N-B-H rocking). Simultaneously, there is an increase in peak intensity at 1635, 1402, 1187, 1165 and 1077cm⁻¹ (grey highlights). This represents a shift of the AB peaks to the higher wavenumber as the PEO content in the fibres increases. A similar, low intensity, shift is observed in the high frequency region. Correspondingly, the PEO peaks at 1096 cm⁻¹ (C-O stretch) and 1279 cm⁻¹ (CH₂ twist) have both split into two overlapping peaks in the AB-PEO fibres at 1105 cm⁻¹ and 1093 cm⁻¹ and 1285 cm⁻¹ and 1275 cm⁻¹ respectively (dashed lines).

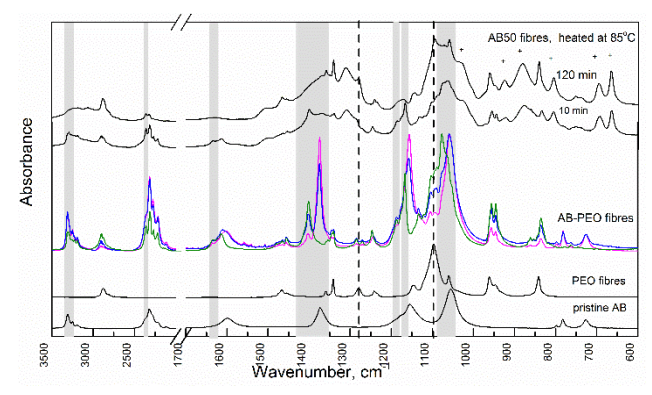


Fig. 8 The FTIR absorption spectra of the pristine AB, electrospun PEO fibres and AB-PEO fibres; AB25 (green), AB50 (blue) and AB750 (pink). Peaks highlighted in

grey indicate a change from AB-AB dihydrogen bonding to AB-PEO hydrogen bonding. Additionally the AB50 fibres have been heated *ex situ* at 85°C, for up to 120 minutes. The peaks (marked +) in the heated AB50 fibres indicate a boron-to-oxygen bond has formed during the dehydrogenation. During heating the boron (AB) and oxygen (PEO) interact.

This suggest that the AB and PEO molecules remain intact in the compound and implies there is some changes in the bonding. Across the fibre samples, the intensity of the new peaks scale with the PEO content and the peak positions are constant. This shows the greatest change in the AB is in the AB25 sample and that the new features present in the fibres represent an ideal, well-defined and preferred arrangement between AB and PEO. The increase in bond vibrational frequency observed indicates a reduction of AB intramolecular bond lengths which correspond to a lengthening and weakening of intermolecular bonds – the dihydrogen bonds. Here it is conceivable that the AB self-to-self dihydrogen bonding is partially replaced by AB-to-PEO hydrogen bonding. Electron donation from the oxygen lone pair to the AB may increase the electron density on the N-H and B-H bonds, shortening them ⁴⁸.

This result is echoed in the ¹¹B and ¹⁵N NMR data. Additional peaks are observed for AB50 fibres as compared to the pristine AB in both spectra, demonstrative of changes in the chemical environment of the nitrogen and boron atoms.

In the ¹⁵N NMR spectra, Fig. 9i, both the pristine AB and the AB50 fibre samples exhibit a strong peak at -366.8 ppm indicative of an NH₃ group. Additionally, the AB50 material displays two small peaks at -371.3 and -374 ppm. These upfield peaks indicate increased shielding around the nitrogen atom of AB in the presence of PEO, suggesting increased electron density at the nitrogen centre. Hydrogen bonding between AB and an etheral oxygen has been recorded previously in literature with 18-crown-6 ether 49 and liquid ethers 23. PEO can be described as a long flexible hydrocarbon chain liberally interspersed with etheral oxygens and therefore it is expected that similar bonding would occur in this case. We therefore suggest that a portion of the electron-deficient nitrogen-bonded hydrogen atoms (H_N) are hydrogen-bonded to the electron-donating oxygen atom in the PEO in preference to boron-bonded hydrogen atoms (H_B). Further, we suggest that the changes observed for the borane group are a knock-on effect owing to the distribution of the increased electron density available on the AB molecule.

ii BH, BH, NH NH, NH, AB50 fibres AB50 fibres pristine AB pristine AB -320-360 -380 -10 -15 -20 -25 -30 ppm ppm

Fig. 9 ¹⁵N (i) and ¹¹B (ii) NMR of pristine AB and AB50 fibres. Additional peaks are observed for AB50 fibres as compared to the pristine AB in both spectra, demonstrative of changes in the chemical environment of the nitrogen and boron atoms. We suggest hydrogen a portion of the AB self-to-self dihydrogen bonding has been replaced by hydrogen bonding between AB and PEO.

In the ¹¹B NMR spectra, Fig. 9ii, the resonances at -28 and -25 ppm are assigned to bulk AB while an extra shoulder at -23 ppm for the AB50 represents, in accordance with the literature, the mobile phase of AB, AB*. This suggests that the presence of the PEO has stabilised a portion of the AB phase into AB*.

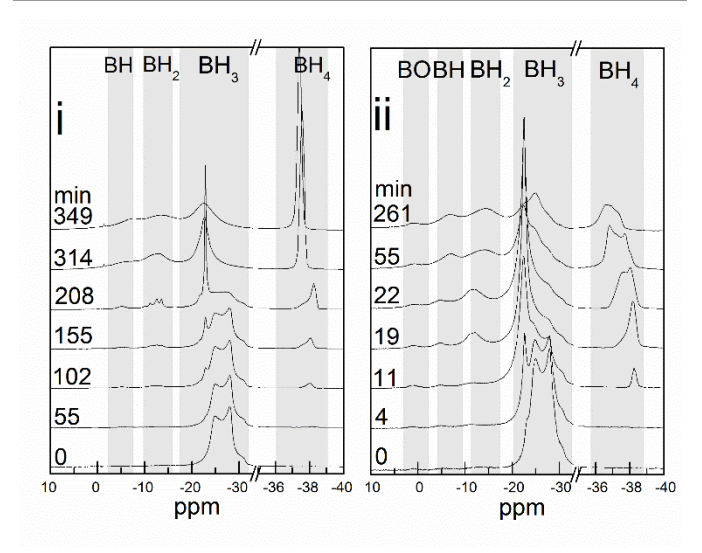


Fig. 10 11 B NMR of pristine AB (i) and 50wt% AB fibres (ii) under 85°C isothermal heating. The time in minutes at which each spectrum was recorded is written above the line

AB* is the precursor to the diammoniate of diborane (DADB) and can be described as a mobile phase of AB with disrupted hydrogen bonding that is distinct from melted AB ^{41,50}. In Fig. 10i, we observe that, for pristine AB at 85°C, an induction period of about 100 minutes precedes the simultaneous appearance of AB* and DADB, BH₄ at -38 ppm and BH₂ -12 ppm. For the AB50 sample in Fig. 10ii under similar conditions, the induction period is eliminated. We suggest the presence of the pregenerated AB* transforms quickly (within 4 minutes) into DADB. As DADB is known to be the precursor of the hydrogen release from AB ⁵⁰, this explains the accelerated

dehydrogenation, related to the PEO content of the AB-PEO fibres observed in Fig. 5 and Fig. 6. If the level of AB* scales with the PEO content in the fibres, this would explain the successive reduction in melting of AB and pellet foaming observed in Fig. 7.

Subsequent heating of AB in Fig. 10i leads the BH₂ peak, previously only representative of DADB, to split into separate peaks at -13.5, -12.5, -11.2 and -9.9 ppm indicating discrete BH₂ environments. These peaks are consistent with the presence of DADB (BH₄ at -38 ppm and BH₂ at -12 ppm) ⁵⁰, linear dimers (NH₃BH₂NH₂BH₃) (terminal BH₃ at -21.7 ppm and BH₂ -12.5 or -11.2 ppm) ⁵⁰ and tentatively polyamido borane (PAB) (BH₂ -11.2 or -9.9 ppm) ⁵¹. In the case of the AB50 fibres in Figure 10ii, a similar peak separation is not evident. This could be the result of the faster dehydrogenation reaction or signify the presence of heterogeneous PAB-type species, perhaps precursors to borazine, in the RGA data 41. Broad signals corresponding to BH groups (-5 ppm) were observed for both the pristine AB and the AB50 sample. The combination of the BH and BH₂ signals suggests either branched B-(cyclodiborazanyl)aminoborohydride (BCDB) or, unlikely at 85°C, polyimidoborane (PIB) 41. The simultaneous presence of several species is reasonable given the nucleation and growth mechanism of AB dehydrogenation and the long timescale of the experiment.

Interestingly, the peak assigned to BH₄ in the ¹¹B NMR spectra (Fig. 10i and ii) is the sum of two peaks, at -37.5 and -38.2 ppm, the latter of which shifts to higher field as the reaction proceeds. A shift to higher field indicates decreased symmetry about the boron atom or weakening of the B-H bonds 52, and this effect is more pronounced in the case of the AB50 fibres. It is likely that there are two distinct BH4 environments, one associated with DADB (-38.2 ppm) and one with PAB moieties (-37.5 ppm). The intensity difference between the two peaks in the pristine AB sample corresponds to the nucleation (short-lived areas of DADB, -38.2 ppm) and propagation (exponentially increasing levels of PAB, -37.5 ppm) of the AB dehydrogenation reaction as observed by Bowden et al. 6. It also supports the nucleation and growth mechanism described by Shaw et al., where PAB chains are constantly lengthened by BH4 working to add other AB molecules but without being used up 41. For the AB50 fibres, the intensities of the two BH4 peaks remain similar throughout the reaction which suggests that the PEO acts to increase the number of nucleation sites for DADB.

Finally, the ¹¹B NMR data of the AB50 sample in Fig. **10**ii display a peak at 1.2 ppm suggesting that a boron-oxygen (B-O) bond is forming during the dehydrogenation of the fibres ⁵³. This is supported by the FTIR spectra of the AB50 fibres at the top of Fig. 8: heating at 85°C is observed to produce a number of new peaks, a significant portion of which (marked +) are identified as stretches of a B-O bond. Considering the proximity of the AB and PEO in the electrospun fibres, an interaction between the electron-donating oxygen atom and the electron-accepting boron atom in AB or one of its decomposition intermediates is highly likely.

Conclusions

The present work shows that electrospinning is an appropriate method for intimately combining AB with PEO to form a new phase which improves the hydrogen release properties of AB significantly, with much reduced incubation time and reduced temperatures for the release of both the 1st and 2nd hydrogen equivalents. This phase can exist due to hydrogen bonding interactions between the ethereal oxygen atom in the PEO and the protic (N-H) hydrogen atoms of AB. This hydrogen bonding between the AB and the polymer replaces the dihydrogen bonding network of the AB, leading to the formation of a mobile AB phase, AB*, which was observed in the NMR spectra at ambient temperatures prior to heating. DADB is known to readily nucleate on AB*, which leads to a significant reduction in the incubation time. Kim et al. showed that polyethers reduce the activation energy of the pathway to DADB, and hence we see a reduction in dehydrogenation onset temperature to 85°C. The reduction of foaming is likely to be the consequence of a lower extent of melting of the AB seen in the DSC. If a portion of the AB is in the form of AB* in the fibres, it is possible that hydrogen release can be initiated below AB melting temperatures. The increased level of borazine release, however, suggests that the PEO encourages AB to follow the cyclic dehydrogenation route over the polymeric route more readily than in pristine AB. The B-O bonds observed in the NMR and FTIR data also play an important role. Either they provide a lower-energy reaction pathway to hydrogen release, or they stabilise the transition of DADB to borazine.

These AB-PEO composites demonstrate several advantages over the AB-PAM and AB-PMA materials. Here, the maximum AB content achieved where a significant reduction in the AB dehydrogenation onset temperature was observed (~15 °C) is, at 75%, far higher than the 20%, 44% and 50% achieved for the AB-PVP ³⁰, AB-PAM ²⁹ and AB-PAA ²⁸ materials respectively. Further, this study also achieved significant control of the foaming and volume expansion of AB which is reduced by a factor of ten in the AB75 sample and further still for the lower AB content fibres. Limiting the expansion of the AB is necessary before it can be employed in a system with a fuel cell. Finally, the presence of ammonia and diborane in the gas stream has been reduced without the need of metal absorbers ^{28,30}. Here we have shown that AB can be used to make a viable 2 solid state hydrogen storage material with a gravimetric hydrogen content of up to 10wt%. PEO has been shown to be a highly promising additive to improve the dehydrogenation properties of AB, paving the way towards safe, lightweight and practical hydrogen storage.

Acknowledgements

The authors would like to acknowledge the technical guidance provided by scientists at Yflow, Malaga, Spain. Thanks also go to Lyndsey Mooring and David Royse for their contributions to this work. Solid state NMR spectra we obtained at the EPSRC

UK National Solid-state NMR Service at Durham. We are grateful to the EPSRC and Cella Energy for funding this work.

Notes and references

- ^a Department of Chemistry, University College London, 20 Gordon Street, London, WC1H 0AJ, UK
- ^b Cella Energy, Rutherford Appleton Laboratory, Harwell Oxford, Didcot, Oxfordshire, OX11 0OX, UK
- ^c Chilton Tech Ltd. Atlas Building, Rutherford Appleton Laboratory, Harwell Oxford, Didcot, Oxfordshire, OX11 0QX, UK

Electronic Supplementary Information (ESI) available: In additional document. See DOI: 10.1039/b000000x/

- F. H. Stephens, V. Pons and R. T. Baker, Dalt. Trans., 2007, 2613.
- S. Satyapal, J. Petrovic, C. Read, G. Thomas and G. Ordaz, *Catal. Today*, 2007, 120, 246.
- 3 E. Mayer, *Inorg. Chem.*, 1972, **11**, 866.
- M. Hu, R. Geanangel and W. Wendlandt, *Thermochim. Acta*, 1978,
 23, 249.
- G. Wolf, J. Baumann, F. Baitalow and F. P. Hoffmann, *Thermochim. Acta*, 2000, 343, 19.
- M. Bowden, T. Autrey, I. Brown and M. Ryan, Curr. Appl. Phys., 2008, 8, 498.
- A. Staubitz, A. P. M. Robertson and I. Manners, *Chem. Rev.*, 2010, 110, 4079
- 8 C. R. Miranda and G. Ceder, J. Chem. Phys., 2007, **126**, 184703.
- D. W. Himmelberger, C. W. Yoon, M. E. Bluhm, P. J. Carroll and L. G. Sneddon, J. Am. Ceram. Soc., 2009, 131, 14101.
- A. C. Gangal, P. Kale, R. Edla, J. Manna and P. Sharma, *Int. J. Hydrogen Energy*, 2012, 37, 6741.
- V. Sit, R. A. Geanangel and W. W. Wendlandt, *Thermochim. Acta*, 1987, **113**, 379.
- A. D. Sutton, A. K. Burrell, D. a Dixon, E. B. Garner, J. C. Gordon,
 T. Nakagawa, K. C. Ott, J. P. Robinson and M. Vasiliu, *Science*,
 2011, 331, 1426.
- G. Moussa, S. Bernard, U. B. Demirci, R. Chiriac and P. Miele, Int. J. Hydrogen Energy, 2012, 37, 13437.
- A. Gutowska, L. Li, Y. Shin, C. M. Wang, X. S. Li, J. C. Linehan, R. S. Smith, B. D. Kay, B. Schmid, W. Shaw, M. Gutowski and T. Autrey, *Angew. Chem. Int. Ed.*, 2005, 44, 3578.
- 15 Z. Tang, H. Chen and X. Chen, J. Am. Chem. Soc., 2012, 134, 5464.

39

40

41

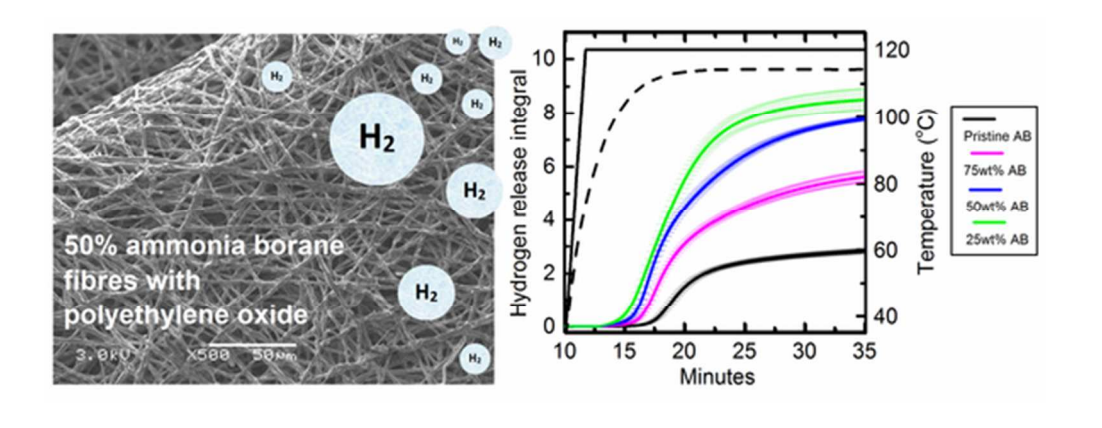
42

Journal Name

16	Z. Kurban, A. Lovell, S. M. Bennington, D. W. K. Jenkins, K. R.	37	Y. J. Choi, I
	Ryan, M. O. Jones, N. T. Skipper and W. I. F. David, J. Phys. Chem.		J. Holladay.
	C, 2010, 21201.		2014, 16 , 79

- K. Chang, E. Kim, P. F. Weck and D. Tománek, *J. Chem. Phys.*, 2011, **134**, 214501.
- 18 G. Srinivas, W. Travis, J. Ford, H. Wu, Z.-X. Guo and T. Yildirim, J. Mater. Chem. A, 2013, 1, 4167.
- 19 S. B. Kalidindi, J. Joseph and B. R. Jagirdar, *Energy Environ. Sci.*, 2009, **2**, 1274.
- 20 M. Chandra and Q. Xu, J. Power Sources, 2006, 156, 190.
- R. J. Keaton, J. M. Blacquiere and R. T. Baker, J. Am. Chem. Soc., 2006, 129, 1844.
- 22 M. C. Denney, V. Pons, T. J. Hebden, D. M. Heinekey and K. I. Goldberg, J. Am. Chem. Soc., 2006, 128, 12048.
- Y. Kim, H. Baek, J. H. Lee, S. Yeo, K. Kim, S.-J. Hwang, B. Eun, S. W. Nam, T.-H. Lim and C. W. Yoon, *Phys. Chem. Chem. Phys.*, 2013, 15, 19584.
- 24 Z. Tang, X. Chen, H. Chen, L. Wu and X. Yu, *Angew. Chemie Int. Ed.*, 2013, **52**, 5832.
- D. J. Heldebrant, A. Karkamkar, N. J. Hess, M. Bowden, S. Rassat, F. Zheng, K. Rappe and T. Autrey, *Chem. Matterials*, 2008, 20, 5332.
- D. W. Himmelberger, L. R. Alden, M. E. Bluhm and L. G. Sneddon, *Inorg. Chem.*, 2009, 48, 9883.
- R. Komm, R. A. Geanangel and R. Liepins, *Inorg. Chem.*, 1983, 22, 1684
- S. F. Li, Z. W. Tang, Y. B. Tan and X. B. Yu, J. Phys. Chem. C, 2012, 116, 1544.
- 29 J. Zhao, J. Shi, X. Zhang, F. Cheng, J. Liang, Z. Tao and J. Chen, Adv. Mater., 2010, 22, 394.
- 30 Z. Tang, S. Li, Z. Yang and X. Yu, J. Mater. Chem., 2011, 21, 14616.
- D. Reneker, A. Yarin, E. Zussman and H. Xu, Adv. Appl. Mech., 2007, 41, 43.
- 32 A. Feaver, S. Sepehri, P. Shamberger, A. Stowe, T. Autrey and G. Cao, *J. Phys. Chem. B*, 2007, **111**, 7469.
- 33 J. Deitzel, *Polymer (Guildf).*, 2001, **42**, 8163.
- P. A. Storozhenko, R. A. Svitsyn, V. A. Ketsko, A. K. Buryak and A. V. Ul'yanov, Russ. J. Iorganic Chem., 2005, 50, 980.
- J. E. Mark, Polymer Data Handbook, Oxford University Press, Oxford, 2nd edn., 2009.
- 36 S. Frueh, R. Kellett, C. Mallery, T. Molter, W. S. Willis, C. King'ondu and S. L. Suib, *Inorg. Chem.*, 2011, 50, 783.

- Y. J. Choi, E. C. E. Rönnebro, S. Rassat, A. Karkamkar, G. Maupin, J. Holladay, K. Simmons and K. Brooks, *Phys. Chem. Chem. Phys.*, 2014, **16**, 7959.
 - F. Baitalow, J. Baumann, G. Wolf, K. Jaenicke-Rößler and G. Leitner, *Thermochim. Acta*, 2002, **391**, 159.
 - F. Merten, G. Wolf and F. Baitalow, in *Handbook of Hydrogen Storage New Materails for Future Energy Storage*, ed. M. Hirscher, Wiley-VCH Verlag GmbH & Co, Weinheim, 2010, 215.
 - J. S. Wang and R. A. Geanangel, *Inorganica Chim. Acta*, 1988, **148**, 185
- W. J. Shaw, J. C. Linehan, N. K. Szymczak, D. J. Heldebrant, C. Yonker, D. M. Camaioni, R. T. Baker and T. Autrey, *Angew. Chemie Int. Ed.*, 2008, **47**, 7493.
 - J. F. Kostka, R. Schellenberg, F. Baitalow, T. Smolinka and F. Mertens, *Eur. J. Inorg. Chem.*, 2012, 49.
- J. Zhang, Y. Zhao, D. Akins and J. Lee, J. Phys. Chem. C, 2011, 115, 8386.
- 44 U. B. Demirci, S. Bernard, R. Chiriac, F. Toche and P. Miele, J. Power Sources, 2011, 196, 279.
- 45 S. Xie, Y. Song and Z. Liu, Can. J. Chem., 2009, 87, 1235.
- 46 N. Gondaliya, Dinesh Kumar Kanchan, P. Sharma and P. Joge, Mater. Sci. Appl., 2011, 2, 1639.
 - M. Sundar and S. Selladurai, Ionics (Kiel)., 2006, 12, 281.
- 48 J. Joseph and E. D. Jemmis, *J. Am. Chem. Soc.*, 2007, **129**, 4620.
- H. M. Colquhoun, G. Jones, J. M. Maud, J. F. Stoddart and D. J. Williams, J. Chem. Soc. Dalt. Trans., 1984, 63.
- A. C. Stowe, W. J. Shaw, J. C. Linehan, B. Schmid and T. Autrey, *Phys. Chem. Chem. Phys.*, 2007, 9, 1831.
- 51 M. E. Bluhm, M. G. Bradley, R. I. Butterick, U. Kusari and L. G. Sneddon, *J. Am. Chem. Soc.*, 2006, **128**, 7748.
- 52 B. Kang and G. Ceder, *Nature*, 2009, **458**, 190.
- 53 S. Sepehri, A. Feaver, W. J. Shaw, C. J. Howard, Q. Zhang, T. Autrey and G. Cao, *J. Phys. Chem. B*, 2007, **111**, 14285.



49x19mm (300 x 300 DPI)